Predicting the moment of inertia of pulsar J0737-3039A from Bayesian modeling of the nuclear equation of state

Yeunhwan Lim,[1,*] Jeremy W. Holt,[1,2,†] and Robert J. Stahulak[3,‡]
[1]*Cyclotron Institute, Texas A&M University, College Station, Texas 77843, USA*
[2]*Department of Physics and Astronomy, Texas A&M University, College Station, Texas 77843, USA*
[3]*Department of Physics and Astronomy, University of Utah, Salt Lake City, Utah 84112, USA*

(Received 13 November 2018; revised manuscript received 22 July 2019; published 16 September 2019)

We investigate neutron star moments of inertia from Bayesian posterior probability distributions of the nuclear equation of state that incorporate information from microscopic many-body theory and empirical data of finite nuclei. We focus on PSR J0737-3039A and predict that for this $1.338\,M_\odot$ neutron star the moment of inertia lies in the range $1.04 \times 10^{45}\,\mathrm{g\,cm^2} < I < 1.51 \times 10^{45}\,\mathrm{g\,cm^2}$ at the 95% credibility level, while the most probable value for the moment of inertia is $\tilde{I} = 1.36 \times 10^{45}\,\mathrm{g\,cm^2}$. Assuming a measurement of the PSR J0737-3039A moment of inertia to 10% precision, we study the implications for neutron star radii and tidal deformabilities. We also determine the crustal component of the moment of inertia and find that for typical neutron star masses $1.3M_\odot < M < 1.5M_\odot$ the crust contributes 1–6% of the total moment of inertia, below what is needed to explain large pulsar glitches in the scenario of strong neutron entrainment.

DOI: 10.1103/PhysRevC.100.035802

I. INTRODUCTION

Neutron star observations are a promising tool [1] to infer the properties of matter at extraordinarily high densities on the order of several times that of atomic nuclei. Shortly after the discovery [2,3] of the double-pulsar system J0737-3039, it was suggested [3,4] that radio timing observations of star A in the pair could lead to a measurement of periastron advance sufficiently precise to resolve the effects of relativistic spin-orbit coupling [5], which enters at second order in a post-Newtonian expansion of the orbital motion. This in turn would place constraints on neutron star moments of inertia [6], complementary to ongoing LIGO/VIRGO gravitational wave observations [7,8] for neutron star tidal deformabilities and X-ray pulsar timing measurements [9] for neutron star radii. All of these efforts aim to shed light on the properties of ultradense matter, its equation of state, and the possible existence of novel phases of matter [10–26] conjectured to exist in the cores of neutron stars.

Several studies [27–32] have already provided a range of predictions for neutron star moments of inertia from different theoretical descriptions of the dense matter equation of state based on (i) nonrelativistic many-body calculations with realistic two- and three-nucleon forces, (ii) nonrelativistic Skyrme effective interactions, (iii) relativistic mean field models, (iv) self-bound strange quarks, and (v) metamodeling that includes only empirical and microscopic constraints on the phenomenological parameters entering in the equation of state. While measurement of a neutron star's moment of inertia to 10% precision may be sufficient [29] to distinguish among several of the qualitatively different models above, a more detailed understanding of the correlations among the moment of inertia, equation of state, neutron star radius, and other bulk neutron star properties can be achieved within a Bayesian statistical framework [32–34]. In previous work [35], we have constructed a model of the dense matter equation of state based on a Taylor series expansion in powers of the Fermi momentum. Bayesian posterior probability distributions for the model parameters were then constructed using microscopic predictions [36–39] from chiral effective field theory [40–45] to define prior probability distribution functions together with empirical data [46,47] for finite nuclei to define likelihood functions. As a first application, we compared the Bayesian modeling of neutron star tidal deformabilities with the first observational data from GW170817 [7].

In the present work we employ the same framework to study the probability distributions for neutron star moments of inertia as a function of mass, focusing on the distribution of values for the $1.338\,M_\odot$ neutron star J0737-3039A. We then make predictions for the crustal fraction of the moment of inertia. This quantity is central to the ongoing debate [31,32,48–51] whether the superfluid angular momentum reservoir in a neutron star inner crust is sufficient to produce the largest pulsar glitches, such as those observed in the Vela pulsar [52]. Previous studies [49,50] that included for the first time a treatment of the neutron band structure in the inner crust have found that the ratio of the crustal moment of inertia to the total moment of inertia may need to be as large as 7–9% in order to account for observed pulsar glitches. In the present work, we find that such large crustal moments of inertia are statistically unlikely in the neutron star mass range 1.2–$1.5\,M_\odot$. Due to competing effects, we find only a minor correlation between the fractional crustal moment of inertia and the core-crust

*ylim@tamu.edu
†holt@physics.tamu.edu
‡r.stahulak@me.com

 ©2019 American Physical Society

transition density, in contrast to previous works [53,54] that suggested a strong correlation with the transition pressure at the crust-core interface.

The paper is organized as follows. In Sec. II we describe the model used to construct the dense matter equation of state and the resulting neutron star composition and structure, including a consistent treatment of the inner crust. In Sec. III we solve the simultaneous equations for hydrostatic equilibrium together with the additional equation for the neutron star moment of inertia in the slow-rotation approximation. In Sec. IV we present our predictions for the probability distribution of neutron star moments of inertia as a function of mass together with correlations among the neutron star radius, tidal deformability, nuclear symmetry energy slope parameter, as well as the core-crust transition density and pressure. We also compute the crustal fraction of the neutron star moment of inertia and the implications for the standard model of pulsar glitches. We end with a summary and conclusions.

II. PARAMETERIZED NUCLEAR ENERGY DENSITY FUNCTIONAL

The nuclear equation of state (EOS), which relates the energy density and pressure at a given baryon number density, is essential for understanding the phenomenology of compact stars. Purely microscopic approaches for computing the cold dense matter equation of state start from realistic nuclear forces fitted to nucleon-nucleon scattering data, the deuteron binding energy, and also the properties of few-nucleon systems when three-body forces are included. Recently there has been much interest [37,39,55–67] in deriving constraints on the equation of state from chiral effective field theory, a framework for constructing the nuclear force that allows for the quantification of theoretical uncertainties through variations in the low-energy constants of the theory, the order in the chiral expansion, and the choice of resolution scale. However, since the typical momentum-space cutoffs used to regularize ultraviolet-divergent loop integrals are on the order of $\Lambda \lesssim 600\,\mathrm{MeV}$, chiral nuclear potentials are not expected to provide a good description of nuclear matter for densities larger than about twice saturation density $2n_0 = 0.32\,\mathrm{fm}^{-3}$. For the lowest-cutoff chiral potential ($\Lambda = 414\,\mathrm{MeV}$) employed in the present work, the breakdown density is expected to be even smaller. Nevertheless, we find it useful and informative to compute the dense matter equation of state up to $n = 0.32\,\mathrm{fm}^{-3}$ for all chiral potentials. Extensions to higher densities are strongly model dependent, but previous works have employed general polytrope extrapolations [68,69] or speed of sound parametrization [70], allowing for the inclusion of phase transitions and general conformal bounds [71] for strongly interacting matter at very high energy densities.

In the present work, we employ a minimal model for the nuclear energy density functional beyond $n > 2n_0$ in which we fit predictions from chiral effective field theory to a fourth-order power series expansion in the Fermi momentum up to $n = 2n_0$ and then extrapolate this functional without modification to larger densities. We therefore do not explore the widest range of high-density equations of state that could include phase transitions or higher powers of the Fermi momentum. The present modeling is therefore expected to be most reliable for neutron stars with $M \lesssim 1.4M_\odot$, where the maximum central density is $n_{\max} \lesssim 3n_0$ [72]. For densities larger than $2n_0$, nucleons begin to overlap and the description in terms of purely hadronic degrees of freedom becomes increasingly questionable. The presence of a phase transition from hadronic to quark matter generically leads to an immediate softening of the equation of state and a reduction in the neutron star radius (and therefore also the moment of inertia), however, the fate of the heaviest neutron stars under hadron-quark phase transitions is strongly model dependent [50,73,74].

One of the primary aims of neutron star observations is to search for indications of novel phases of strongly interacting matter in neutron star cores, and the minimal model employed in the present study provides a useful baseline scenario without exotic degrees of freedom or phase transitions. Specifically we write the energy density as

$$\mathcal{E}(n,\delta) = \frac{1}{2m}\tau_n + \frac{1}{2m}\tau_p + [1-\delta^2]f_s(n) + \delta^2 f_n(n), \quad (1)$$

where $\delta = \frac{n_n - n_p}{n}$ is the isospin asymmetry, τ_p and τ_n are the proton and neutron kinetic densities, and f_s and f_n are the potential energy contributions for symmetric nuclear matter and pure neutron matter of the form

$$f_s(n) = \sum_{i=0}^{3} a_i\, n^{(2+i/3)}, \quad f_n(n) = \sum_{i=0}^{3} b_i\, n^{(2+i/3)}. \quad (2)$$

The coefficients a_i and b_i are fitted to individual symmetric nuclear matter and pure neutron matter equations of state computed in many-body perturbation theory using chiral nuclear forces up to $n = 2n_0$. We have found that the values of the expansion parameters do not depend strongly on the choice of maximal density. For instance, in previous works [35,75] we have reduced the maximum density of the fitting range to $n = 0.25\,\mathrm{fm}^{-3}$ and found only small quantitative differences in the fitting parameters and derived probability distributions. We include ten equations of state obtained by varying the chiral order of the nucleon-nucleon potential from next-to-next-to-leading order (N2LO) to N3LO, the order in many-body perturbation theory from second to third order, and finally the momentum-space cutoff from $\Lambda \simeq 400$–$500\,\mathrm{MeV}$. The mean and covariance matrices for $\{a_i\}$ and $\{b_i\}$ then define our prior Gaussian probability distributions.

Since none of the adjustable parameters in chiral nuclear potentials are explicitly fitted to the properties of nuclear matter, we then incorporate empirical constraints on the nuclear matter equation of state into Bayesian likelihood functions involving the $\{a_i\}$ and $\{b_i\}$ parameters. For symmetric nuclear matter, we consider the saturation density n_0, saturation energy B, incompressibility K, and skewness Q. The values for these quantities are typically obtained from fitting energy density functionals to the binding energies and charge radii of finite nuclei. We consider 205 high quality models [46], which give the average and standard deviations $n_0 = 0.160 \pm 0.003\,\mathrm{fm}^{-3}$, $B = 15.939 \pm 0.149\,\mathrm{MeV}$, $K = 232.65 \pm 7.00\,\mathrm{MeV}$, $Q = -373.26 \pm 13.91\,\mathrm{MeV}$. The parameters $\{a_i\}$ are then uniquely determined in terms of

the empirical nuclear matter parameters $\{n_0, B, K, Q\}$, which provides a method to derive Bayesian likelihood functions involving the a_i. Note that we choose 205 Skyrme force models among 240 considered in Ref. [46]. Some of these Skyrme models do not reproduce the well known nuclear matter properties at saturation density. For instance, Skyrme models for which $n_0 < 0.15\,\mathrm{fm}^{-3}$, $B < 15\,\mathrm{MeV}$, $B > 17\,\mathrm{MeV}$, and $K > 300\,\mathrm{MeV}$ have been omitted. We note that the statistical uncertainty in some empirical parameters, especially Q, come out rather small when computed over the 205 Skyrme forces. However, we have doubled the standard deviations on both K and Q and found only small quantitative changes on the order of <1% to the neutron star properties computed below.

For pure neutron matter there are no strong empirical constraints on the equation of state. However, the nuclear symmetry energy $E_{\mathrm{sym}} = \frac{E}{A}(n, \delta = 1) - \frac{E}{A}(n, \delta = 0)$ is closely related to the isospin asymmetry energy $J = \frac{1}{2}\frac{\partial E/A}{\partial \delta^2}|_{\delta=0, n=n_0}$, which can be extracted from the binding energies of nuclei, giant dipole resonances, neutron skin thicknesses, and heavy-ion collision flow data. Recent analyses [76,77] give $J = 31 \pm 1.5\,\mathrm{MeV}$. For comparison we note that the range of theoretical predictions for the pure neutron matter equation of state at saturation density derived from our chiral EFT calculations is $E/A = 13.8$–$19.7\,\mathrm{MeV}$, corresponding to values of the symmetry energy in the range $29.5\,\mathrm{MeV} \leqslant E_{\mathrm{sym}} \leqslant 36.0\,\mathrm{MeV}$, conservatively assuming $B = 16.0 \pm 0.3\,\mathrm{MeV}$. In addition, the 205 selected Skyrme forces give the range $\langle J \rangle = 31.3\,\mathrm{MeV}$, $\sigma_J = 6.6\,\mathrm{MeV}$, which is larger than that obtained from a comprehensive analysis of nuclear experimental data in Refs. [76,77]. From correlations [47,78] among the isospin asymmetry energy J, its slope parameter L and curvature K_{sym}, likelihood functions involving the b_i were obtained in Ref. [35] to derive the final Bayesian posterior probability distributions. Figure 1 shows the J and L distribution of the Bayesian modeling in the present work. Both J and L have their own Gaussian-like distributions, but there exists a strong correlation between J and L that can be seen also in nuclear mass model calculations [76,79]. In this work, we obtain $29.1\,\mathrm{MeV} \leqslant J \leqslant 34.4\,\mathrm{MeV}$ and $34.6\,\mathrm{MeV} \leqslant L \leqslant 72.6\,\mathrm{MeV}$, with the correlation $R_{JL} = 0.93$ and the slope $\tan\alpha = 7.94$, from our Bayesian posterior probability distributions.

Randomly sampling from the a_i and b_i joint probability distributions, we construct 300 000 equations of state for nuclear matter in beta equilibrium. For the crust EOS, we utilize a liquid drop model with the same nuclear model used in the bulk matter equation of state [80]. This provides a unified approach, since the structure is constructed by a single nuclear model, without the need to stitch together various bulk matter EOSs with one specific crust EOS. Since we use the same nuclear force model for both the core and crust, the core-crust density is treated consistently, and therefore the moment of inertia from the crust can be calculated correctly.

In the liquid drop model at $T = 0\,\mathrm{MeV}$, the total energy density is given by [81,82]

$$\varepsilon = un_i f_i + \frac{\sigma(x_i) u d}{r_N} + 2\pi (n_i x_i e r_N)^2 u f_d(u) + (1-u) n_{no} f_{no}, \tag{3}$$

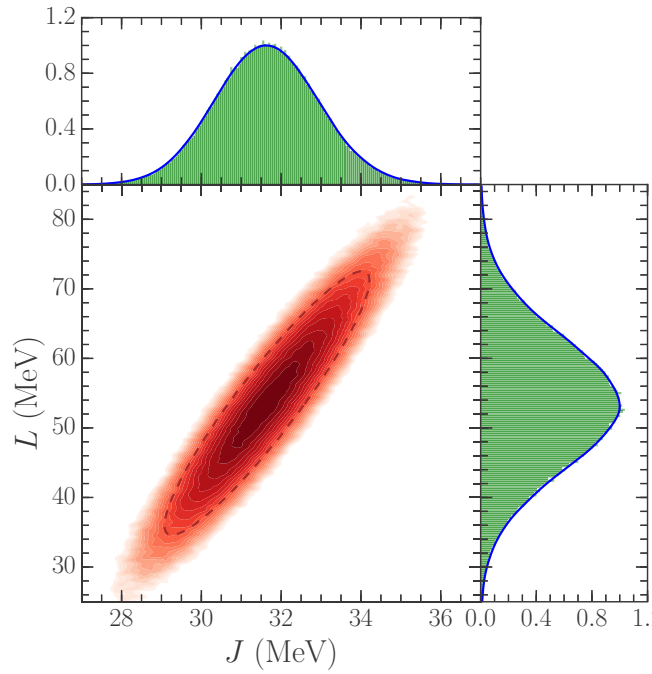

FIG. 1. Distribution of nuclear symmetry energy and its density slope at the nuclear saturation density from the Bayesian modeling in this work.

where u is the volume fraction of a heavy nucleus in the Wigner-Seitz cell, n_i is the baryon number density of the heavy nucleus, f_i is the energy density of the heavy nucleus, $\sigma(x_i)$ is the surface tension as a function of proton fraction (x_i) of the heavy nucleus, d is the dimension of the nuclear phase (e.g., spherical, cylindrical, or slab), r_N is the radius of the heavy nucleus, $f_d(u)$ is the geometric function that reflects the nuclear pasta phase, n_{no} is the neutron density outside of the heavy nucleus, and f_{no} is the energy density of the neutron gas. The nuclear configuration is determined by minimizing the energy density for a given total baryon number density n and proton fraction x. In β equilibrium matter, we include electrons and find the proton (or electron) fraction x that minimizes the total energy density. Note that we use the same energy density functional for f_i and f_{no} as used in the bulk matter EOS. By applying the Lagrange multiplier method with the constraints for baryon and charge number density, we have [82]

$$\begin{aligned} \mu_{ni} - \frac{x_i \sigma'(x_i) d}{r_N n_i} &= \mu_{\mathrm{no}}, \\ p_i - 2\pi (n_i x_i e r_N)^2 \frac{\partial (u f_d)}{\partial u} &= p_{\mathrm{no}}, \\ n - u n_i - (1-u) n_{no} &= 0, \\ nx - u n_i x_i &= 0. \end{aligned} \tag{4}$$

The core-crust transition density is found by comparing the energy density of inhomogeneous matter and uniform nuclear matter. Near the phase boundaries, we employ a Maxwell construction to find the exact density and pressure,

$$p_{\mathrm{inh.}} = p_{\mathrm{uni.}}, \quad \mu_{n_{\mathrm{inh.}}} = \mu_{n_{\mathrm{uni.}}}, \tag{5}$$

where "inh." (uni.) stands for inhomogeneous (uniform) matter.

III. MOMENT OF INERTIA

The neutron star mass and radius are obtained by solving the Tolman-Oppenheimer-Volkov (TOV) equation, which is the hydrostatic equilibrium equation for spherically symmetric neutron stars, given by

$$\frac{dp}{dr} = -\frac{(\varepsilon + p)(m + 4\pi r^3 p)}{r(r - 2m)}, \tag{6a}$$

$$\frac{dm}{dr} = 4\pi r^2 \varepsilon, \tag{6b}$$

where p is the pressure, ε is the energy density (including rest mass), and m is the enclosed mass within the distance r from the center. The neutron star moment of inertia is then calculated by solving the conventional TOV equation with an additional equation including the rotational frequency. In a slowly rotating neutron star, the moment of inertia is given by [83,84]

$$I = \frac{8\pi}{3}\int_0^R r^4(\varepsilon + p)e^{(\lambda-\nu)/2}\frac{\bar{\omega}}{\Omega}\,dr, \tag{7}$$

where λ and ν are metric functions defined by

$$e^{-\lambda} = \left(1 - \frac{2m}{r}\right)^{-1}, \tag{8}$$

$$\frac{d\nu}{dr} = -\frac{2}{\varepsilon + p}\frac{dp}{dr}, \tag{9}$$

Ω is the angular velocity of a uniformly rotating neutron star, and $\bar{\omega}$ is the rotational drag function. The unitless frequency $\tilde{\omega} = \frac{\bar{\omega}}{\Omega}$ satisfies

$$\frac{d}{dr}\left(r^4 j\frac{d\tilde{\omega}}{dr}\right) = -4r^3\tilde{\omega}\frac{dj}{dr}, \tag{10}$$

where $j = e^{-(\lambda+\nu)/2}$. This rotational drag $\tilde{\omega}$ meets the boundary conditions

$$\tilde{\omega}(r = R) = 1 - \frac{2I}{R^3} \quad \text{and} \quad \left.\frac{d\tilde{\omega}}{dr}\right|_{r=0} = 0 \tag{11}$$

at the surface and center of the neutron star. The moment of inertia can be integrated from

$$I = \frac{2}{3}\int_0^R r^3\,\tilde{\omega}\frac{dj}{dr}\,dr = \frac{1}{6}\int_0^R \frac{d}{dr}\left(r^4 j\frac{d\tilde{\omega}}{dr}\right)dr$$
$$= \left.\frac{R^4}{6}\frac{d\tilde{\omega}}{dr}\right|_{r=R}. \tag{12}$$

The second-order differential Eq. (10) can be translated to a first-order differential equation by introducing $\phi = d\ln\tilde{\omega}/d\ln r$, giving

$$\frac{d\phi}{dr} = -\frac{\phi}{r}(\phi + 3) - (4 + \phi)\frac{d\ln j}{dr}$$
$$= -\frac{\phi}{r}(\phi + 3) + (4 + \phi)\frac{4\pi r^2(\varepsilon + p)}{(r - 2m)}, \tag{13}$$

with the boundary condition

$$\phi(r = 0) = 0. \tag{14}$$

The total moment of inertia of a neutron star is then given as

$$I = \frac{R^3}{6}\phi_R\tilde{\omega}_R = \frac{\phi_R}{6}(R^3 - 2I), \quad I = \frac{R^3\phi_R}{6 + 2\phi_R}, \tag{15}$$

with the boundary condition in Eq. (11).

The moment of inertia of the core is given by integrating Eq. (12) up to the core radius $r = R_t$:

$$I_c = \left.\frac{R_t^4}{6}\frac{d\tilde{\omega}}{dr}\right|_{r=R_t} = \frac{R_t^3}{6}\phi_t\tilde{\omega}_t. \tag{16}$$

From the relation between ϕ and $\tilde{\omega}$, we have

$$\tilde{\omega}_t = \tilde{\omega}_R\,\mathrm{Exp}\left[-\int_{R_t}^R \frac{\phi(r)}{r}\,dr\right]. \tag{17}$$

Thus, the moment of inertia of the crust is given as

$$\Delta I = I - I_c = \frac{R^3}{6}\phi_R\tilde{\omega}_R\left[1 - \left(\frac{R_t}{R}\right)^3\frac{\phi_t}{\phi_R}\frac{\tilde{\omega}_t}{\tilde{\omega}_R}\right]$$
$$= I\left\{1 - \left(\frac{R_t}{R}\right)^3\frac{\phi_t}{\phi_R}\,\mathrm{Exp}\left[-\int_{R_t}^R \frac{\phi(r)}{r}\,dr\right]\right\}. \tag{18}$$

It is known that the slow rotation approximation is valid for J0737-3039A by comparing to the exact numerical solution without approximation [29]. The error between the exact solution and slow rotation approximation is estimated by $(\Omega/\Omega_{\max})^2$ where $\Omega_{\max} \approx (GM/R^3)^{1/2}$ is the Kepler frequency at the equator of neutron stars. For a neutron star with $1.4\,M_\odot$ with 12 km radius, the Kepler frequency is around 7.9×10^3 Hz. Thus, it is expected that for most millisecond pulsars the slow rotation approximation is valid.

IV. RESULTS

In the present section we analyze 300 000 equations of state randomly sampled from the Bayesian posterior distributions for the a_i and b_i parameters entering into the nuclear energy density functional of Eq. (1). For each equation of state we consider up to 110 representative neutron stars with masses in the range $1.0M_\odot \leqslant M \leqslant 2.1M_\odot$ with spacing $\Delta M = 0.01M_\odot$. In the case that the particular equation of state yields a maximum mass such that $M_{\max} < 2.1M_\odot$, which occurs for the softest equations of state generated, we use the same mass spacing but with a modified range $1.1M_\odot \leqslant M \leqslant M_{\max}$. In total we therefore consider more than 30 000 000 neutron stars for analysis, each constructed with a realistic crust equation of state.

In Fig. 2 we show in red the resulting probability distribution for the ratio of the moment of inertia I to MR^2 as a function of M/R. In the previous work [4] it was shown that in the absence of phase transitions and other effects that strongly soften the equation of state beyond a few times normal nuclear densities, there is a nearly unique relation between the quantity I/MR^2 and M/R. This relation is shown as the blue band in Fig. 2 which we have generated from the empirical formula obtained in Ref. [4]. Observational evidence suggests that

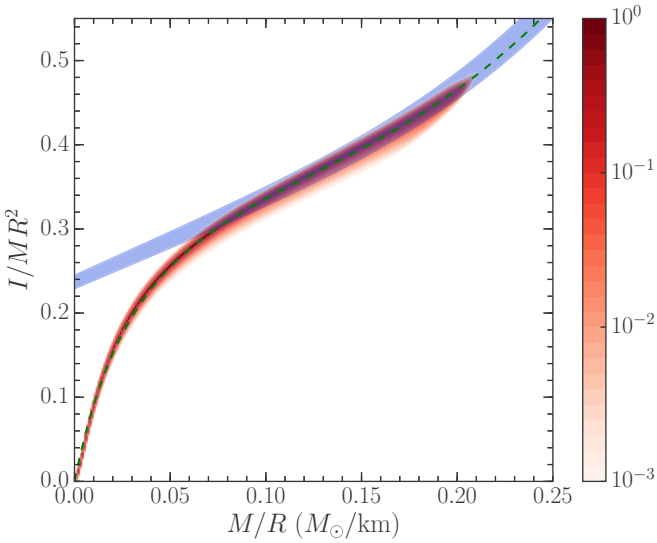

FIG. 2. Probability distribution (red) for the ratio of the neutron star moment of inertia I to MR^2 as a function of the compactness parameter M/R. The distribution is obtained by randomly sampling 300 000 configurations from the Bayesian posterior probability distributions. The empirical (blue) band from Ref. [4] is shown together with the fitting function (green dotted) in Eq. (19).

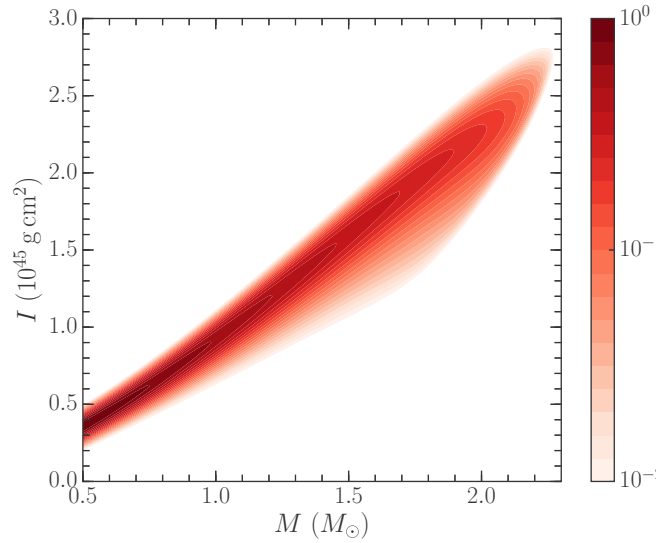

FIG. 3. Probability distribution for the neutron star moment of inertia as a function of its mass from the 300 000 equations of state randomly sampled from the Bayesian posterior distribution.

neutron star masses lie in the range $1.2\,M_\odot \leqslant M \leqslant 2.0\,M_\odot$ while radii lie in the range $9\,\mathrm{km} \leqslant R \leqslant 15\,\mathrm{km}$. Therefore, we expect only the region $0.08\,\frac{M_\odot}{\mathrm{km}} < M/R < 0.22\,\frac{M_\odot}{\mathrm{km}}$ to be physically relevant. For this range of neutron star compactness parameters $C = M/R$ our results are completely consistent with the empirical relation in Ref. [4]. We find that over the entire range of neutron star compactnesses, the following formula holds:

$$\frac{I}{MR^2} = \frac{M/R + a(M/R)^4}{b + c(M/R)}, \tag{19}$$

where $a = 27.178\,(M_\odot/\mathrm{km})^{-3}$, $b = 0.0871\,M_\odot/\mathrm{km}$, and $c = 2.183$. This formula is shown as the green dotted curve in Fig. 2 and should be accurate for most neutron star configurations. The relative error for $M/R = 0.01\,M_\odot/\mathrm{km}$ ($M/R = 0.213\,M_\odot/\mathrm{km}$) is 3.2% (1.05%). In the case of $M = 1.44\,M_\odot$, $R = 12\,\mathrm{km}$, which is the canonical average of neutron stars, the relative error is only 0.06%.

In Fig. 3 we show the neutron star moment of inertia as a function of mass, plotted as a probability distribution based on the 300 000 equations of state sampled from our Bayesian posterior distribution. Naturally the moment of inertia increases approximately linearly with the mass. The uncertainty also generically increases with the neutron star mass up to about $M \simeq 1.8 M_\odot$. Beyond this value, the fraction of equations of state capable of producing such massive neutron stars decreases as does the range of allowed radii for a given mass. This results in a narrowing of the moment of inertia probability distribution for the largest-mass neutron stars in our sample.

From Fig. 2 we see that a simultaneous measurement of neutron star mass and moment of inertia will indeed strongly constrain the radius. This is demonstrated more explicitly in Fig. 4, where we plot the probability distribution for the neutron star moment of inertia versus neutron star radius for a fixed mass of $M = 1.338 M_\odot$ corresponding to that of PSR J0737-3039A. A total of 300 000 samples are considered, one for each of the generated equations of state. We see that the moment of inertia lies in the range $1.04 \leqslant I_{45} \leqslant 1.51$ (95% credibility), where for convenience we have defined $I \equiv I_{45} \times 10^{45}\,\mathrm{g\,cm^2}$, while the radius lies between $10.3\,\mathrm{km} \leqslant R \leqslant 12.9\,\mathrm{km}$ (95% credibility). In addition we observe an approximate linear correlation between the moment of inertia

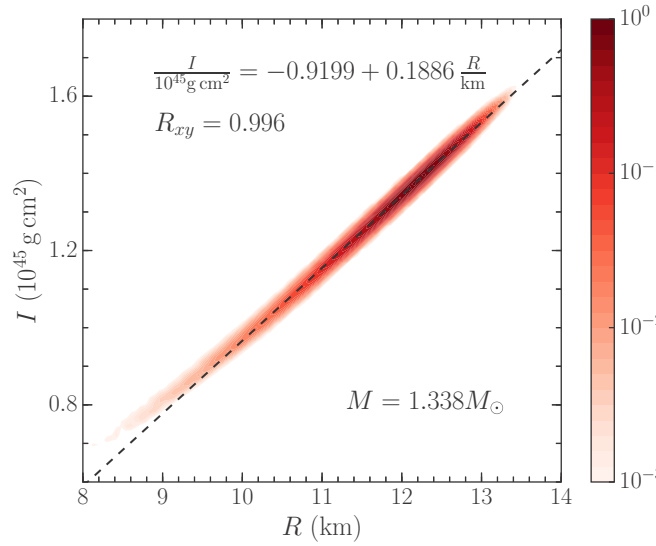

FIG. 4. Probability distribution (red) for the neutron star moment of inertia vs. radius at a fixed mass of $M = 1.338\,M_\odot$ from a Bayesian analysis of the nuclear equation of state. The empirical relation is shown as a black dashed line.

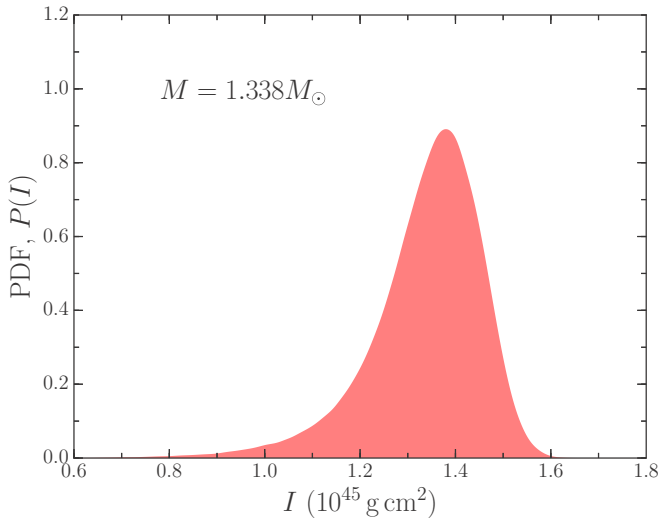

FIG. 5. Probability distribution for the moment of inertia of a $1.338 M_\odot$ neutron star based on the energy density functionals constrained by nuclear theory and experiment.

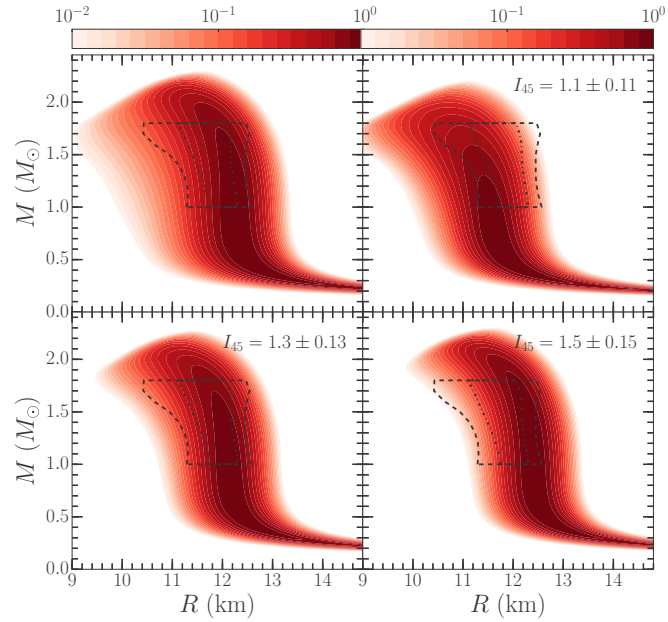

FIG. 6. Posterior probability distributions for the neutron star mass vs. radius relation from artificial moment of inertia measurements with 10% uncertainties.

and the radius in this regime of the form

$$I = \left(-0.9199 + 0.1886 \frac{R}{\mathrm{km}}\right) \times 10^{45}\,\mathrm{g\,cm^2} \qquad (20)$$

with correlation coefficient $R = 0.996$. From Fig. 4 we observe that the moment of inertia probability distribution is asymmetric and peaks around $I \simeq 1.36 \times 10^{45}\,\mathrm{g\,cm^2}$ and $R \simeq 12.2\,\mathrm{km}$. We present in Fig. 5 the full probability distribution function for the moment of inertia of a $1.338 M_\odot$ neutron star from the 300 000 EOSs constructed in this work. The probability function appears as an asymmetric Gaussian function and therefore the average value of the total moment of inertia $\langle I \rangle$ does not match the most probable moment of inertia, which we denote by $\tilde{I}$. In this work, we find $\langle I \rangle = 1.338 \times 10^{45}\,\mathrm{g\,cm^2}$ with one- and two-sigma credibility ranges given by $I_{-\sigma} = 1.233$, $I_{+\sigma} = 1.443$, $I_{-2\sigma} = 1.035$, and $I_{+2\sigma} = 1.514$ in units of $10^{45}\,\mathrm{g\,cm^2}$. In comparison the most likely value of the moment of inertia is found to be $\tilde{I} = 1.355 \times 10^{45}\,\mathrm{g\,cm^2}$.

A precise moment of inertia measurement to 10% precision is expected to be competitive with gravitational wave constraints on neutron star radii [8] as well as direct measurements of radii from x-ray observations. We now discuss the implications for such a moment of inertia measurement and how it can be implemented in the current Bayesian modeling of the equation of state. In the top left panel of Fig. 6 we show the neutron star mass and radius distribution resulting from our Bayesian analysis of the nuclear energy density functional including constraints from microscopic many-body theory and nuclear experiments. The softest equations of state generated from the statistical sampling do not reach a maximum neutron star mass of $M_{\mathrm{max}} = 2M_\odot$, but this is due primarily to our smooth continuation of the equation of state beyond twice saturation density. In particular we cannot rule out the existence of higher-power repulsive contributions to the nuclear energy density functional beyond $n > 2n_0$ that might sufficiently stiffen the equations of state to support a $2M_\odot$ neutron star. In the present work we do not focus on the properties of the heaviest neutron stars and therefore we keep the softest equations of state in our subsequent analysis.

As the value of the neutron star moment of inertia I increases, so too does the statistical average of the neutron star radius. Our current EOS distribution results in $\langle R \rangle = 12.01\,\mathrm{km}$, $R_{-\sigma} = 11.36\,\mathrm{km}$, $R_{+\sigma} = 12.48\,\mathrm{km}$, $R_{-2\sigma} = 10.26\,\mathrm{km}$, $R_{+2\sigma} = 12.87\,\mathrm{km}$ for a $1.4\,M_\odot$ neutron star, and the most probable radius is $\tilde{R} = 12.15\,\mathrm{km}$. We apply Bayesian analysis to see how the credibility interval varies for a given moment of inertia measurement. Bayesian statistics gives for the posterior probability

$$P(\mathcal{M}_i|D) = \frac{P(D|\mathcal{M}_i)P(\mathcal{M}_i)}{\sum_j P(D|\mathcal{M}_j)P(\mathcal{M}_j)}, \qquad (21)$$

where $\mathcal{M}_i$ stands for the nuclear model parameters, D represents the data set, $P(\mathcal{M}|D)$ is the posterior probability, $P(D|\mathcal{M})$ is the likelihood function, and $P(\mathcal{M})$ is the prior distribution function, which in this case we take to be that arising from the inclusion of EOS constraints from nuclear theory and experiment (that is, our previous posterior distribution function). From n measurements of the moment of inertia I_k and the corresponding uncertainties σ_k, we define the likelihood function for a specific nuclear model as

$$P(D|\mathcal{M}) = \prod_k^n \frac{1}{\sqrt{2\pi}\sigma_k} \mathrm{Exp}\left[-\frac{(I(\mathcal{M}) - I_k)^2}{2\sigma_k^2}\right], \qquad (22)$$

where $I(\mathcal{M})$ is the moment of inertia from the specific nuclear model.

In the top-right, bottom-left, and bottom-right panels of Fig. 6 we show the resulting posterior probability distribution

TABLE I. Bayesian analysis for the radius of a $1.4\,M_\odot$ neutron star from artificial moment of inertia measurements at 10% precision for three different cases.

	$R_{-2\sigma}$ (km)	$R_{-\sigma}$ (km)	$\tilde{R}$ (km)	$R_{+\sigma}$ (km)	$R_{+2\sigma}$ (km)
–	10.26	11.36	12.15	12.48	12.87
I^1_{45}	9.97	10.64	11.35	11.76	12.20
I^2_{45}	10.89	11.46	12.05	12.35	12.71
I^3_{45}	11.33	11.82	12.30	12.61	12.93

for the neutron star mass-radius relation assuming the following moment of inertia measurements for the $1.338\,M_\odot$ neutron star in PSR J0737-3039: $\{I^1_{45} = 1.1 \pm 0.11,\ I^2_{45} = 1.3 \pm 0.13,\ I^3_{45} = 1.5 \pm 0.15\}$. The resulting 1σ and 2σ credibility intervals for the radius of a $1.4\,M_\odot$ neutron star are shown in Table I. For instance, in the case that $I^1_{45} = 1.1 \pm 0.11$, the maximum radius for a $1.4\,M_\odot$ neutron star would be shifted down to approximately $R_{\rm max} \simeq 12.2\,$km. Likewise, under the scenario where $I^3_{45} = 1.5 \pm 0.15$ the minimum radius would be shifted up to about $R_{\rm min} \simeq 11.3\,$km. Even a moment of inertia measurement nearly consistent with our most probable value from the prior distribution will further constrain the equation of state. This is shown in the lower-left panel of Fig. 6, where a measured value of $I^2_{45} = 1.3 \pm 0.13$ increases the lower bound on the radius of $1.4\,M_\odot$ neutron star up to roughly 10.9 km, even though the measured value of I would be only a few percent below that of the most probable value from the prior distribution.

Even more strongly constraining is the relation between the neutron star moment of inertia and dimensionless tidal deformability as pointed out in Ref. [85]. In Fig. 7 we show the correlation between the tidal deformability and the moment

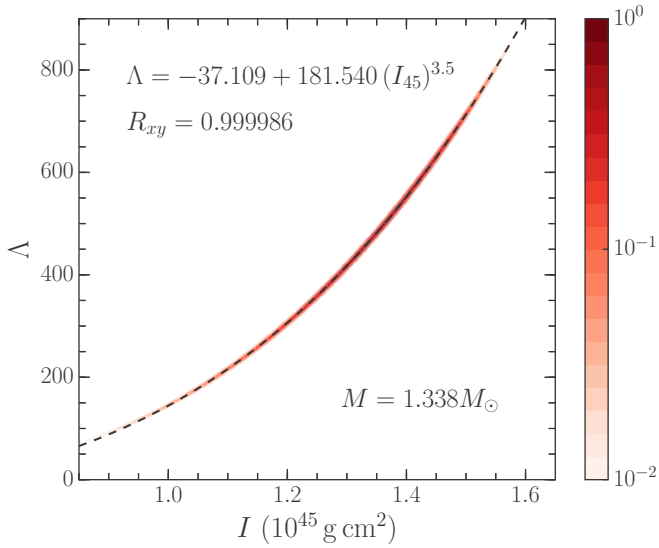

FIG. 7. Probability distribution for the tidal deformability vs. moment of inertia for a neutron star with $M = 1.338\,M_\odot$ obtained from the Bayesian posterior probability distribution constrained by nuclear theory and experiment.

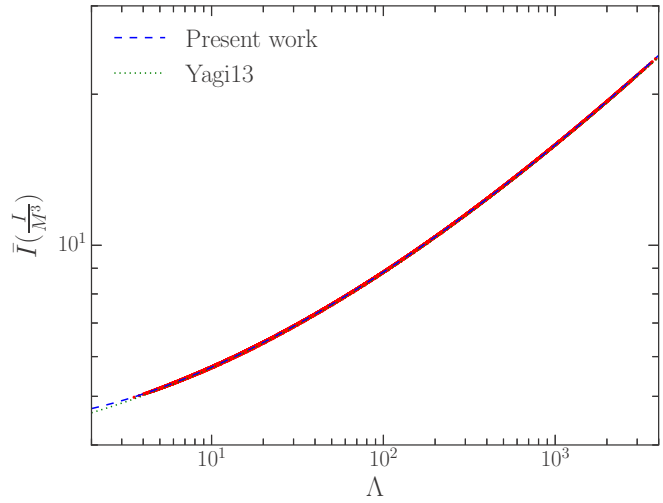

FIG. 8. Distribution (red) for $\bar{I} = I/M^3$ vs. the neutron star tidal deformability Λ. The blue-dashed line is the empirical relation Eq. (24) derived in the present work, and the green-dotted curve is that from Ref. [85].

of inertia of a neutron star with mass $M = 1.338\,M_\odot$. We find the empirical formula,

$$\Lambda = -37.109 + 181.540(I_{45})^{3.5}, \quad \text{for } M = 1.338\,M_\odot. \tag{23}$$

Note that this formula may support different values for the coefficients when neutron stars with different masses are considered, due to the fact that the most probable values of I and Λ vary with the mass. As seen in Fig. 7 precise measurements of neutron star moments of inertia can be used to very tightly constrain the tidal deformability, and vice versa.

In Fig. 8 we demonstrate the strong correlation between $\bar{I} = I/M^3$ and Λ for all of the neutron stars that may be constructed from our Bayesian posterior probability distribution for the nuclear equation of state. The red solid line in Fig. 8 results from plotting individually the scaled moments of inertia versus tidal deformabilities Λ. The log-log functional relationship between $\bar{I}$ and Λ can be well approximated by

$$\mathrm{Log}_{10}(\bar{I}) = 0.65974 + 0.097374[\mathrm{Log}_{10}(\Lambda)]^{1.56}. \tag{24}$$

This is shown as the blue dashed line in Fig. 8. In comparison we also show as the green dashed line in Fig. 8, the original correlation derived in Ref. [85]. While both functions fit the theoretical results very well, we find that our functional form has a smaller χ^2 value with fewer parameters.

Finally, we investigate the fraction of the neutron star moment of inertia contained in the crust. This quantity is related to the ratio of the superfluid angular momentum to the total angular momentum in the neutron star, which must be sufficiently large in order to support the observed glitch activity of the Vela pulsar. One can derive [53] that in the standard hydrodynamic two-fluid model, the ratio of the crustal moment of inertia ΔI to the total moment of inertia I must satisfy

$$\frac{\Delta I}{I} \geqslant 0.014. \tag{25}$$

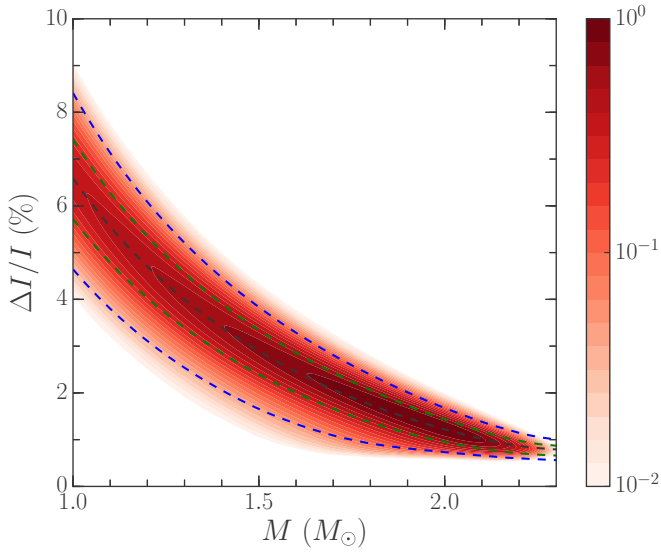

FIG. 9. Probability distribution for the ratio of the crust moment of inertia to the total moment of inertia as a function of the neutron star mass. The most likely value is represented by the black dashed line, while the green- and blue-dashed lines represent the 1σ and 2σ credibility intervals, respectively.

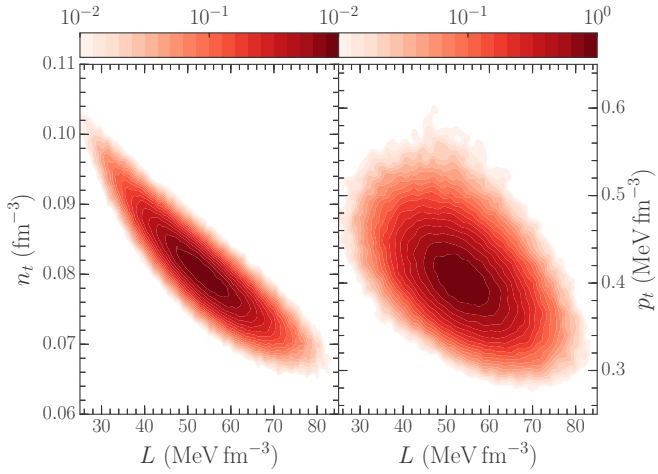

FIG. 10. Contour plot of transition density and transition pressure at the core-crust boundary as a function of the symmetry energy slope parameter L at nuclear saturation density.

However, strong entrainment of otherwise free neutrons by the inner crust can be studied within band theory calculations and has been shown [48–50] to reduce the neutron superfluid angular momentum reservoir. The key quantity is the neutron effective mass, defined as [50]

$$m_n^* \equiv m_n n_n^f / n_n^c, \tag{26}$$

where m_n is the bare neutron mass, n_n^c is the density of conduction neutrons, and n_n^f is the density of unbound neutrons. The neutron effective mass strongly depends on the density and peaks at a value of $m_n^* \simeq 10\, m_n$ around $n = 0.025\,\mathrm{fm}^{-3}$. Averaging over typical densities in the crust leads to a decrease in the superfluid angular momentum reservoir such that $\Delta I/I \gtrsim 0.07$ is required to explain observed glitch activity. Such large crustal moments of inertia are not favored in most theoretical modeling of neutron star structure, especially for the moderately soft equations of state produced by chiral effective field theory.

In Fig. 9 we show the fraction of the crustal moment of inertia to the total moment of inertia as a function of the neutron star mass. The crust moment of inertia is obtained numerically from the Eq. (18). The blue (green) dashed curves in Fig. 9 indicate $\pm 2\sigma$ ($\pm 1\sigma$) credibilities, while the black dashed curve represents the central value of the momentum fraction. Low-mass neutron stars tend to have thicker crusts than high-mass neutron stars, leading to fractional crustal moments of inertia that are systematically larger. Although the mass of the Vela pulsar is not precisely known, recent work [86] has estimated a value $M = 1.51 \pm 0.04\, M_\odot$. From Fig. 9 we see that the present EOS modeling within the scenario of strong neutron entrainment would be insufficient to explain large pulsar glitch activity. However, such large entrainment effects have recently been called into question, and in particular the inclusion of neutron pairing in band theory calculations may significantly reduce neutron entrainment and increase the angular momentum reservoir [51]. In our models, $\Delta I/I \simeq 1.8$–3.9% for a $1.5\, M_\odot$ neutron star, and therefore a reduction in the average neutron entrainment in the crust from $n_n^f/n_n^c \simeq 5$ in the scenario of strong entrainment to $n_n^f/n_n^c \to 1.0$–2.8 would be sufficient to explain the glitch activity of the Vela pulsar.

Connecting the crustal fraction of the moment of inertia to specific features of the nuclear equation of state is challenging. It has been suggested [53,54] that the pressure of beta-equilibrium matter at the neutron star core-crust interface is strongly correlated with the crustal moment of inertia:

$$\Delta I \sim R_t^6\, p_t, \tag{27}$$

where R_t is the radius of the neutron star core and p_t is the pressure at the core-crust boundary. Eq. (27) can be derived under the approximation of slow rotation and thin, low-density crusts. In Fig. 10 we plot the probability contour plot of the crustal density n_t and corresponding pressure p_t at the core-crust interface as a function of the nuclear symmetry energy slope parameter $L = 3n_0 \frac{\partial E_{\mathrm{sym}}}{\partial n}|_{n_0}$. We note here the negative correlation between n_t and L, as well as a weaker negative correlation between p_t and L. This negative correlation results in a related negative correlation between n_t and $\Delta I/I$ and almost no correlation between p_t and $\Delta I/I$ as shown in the right panels of Fig. 11, plotted for a neutron star with mass $M = 1.338 M_\odot$. That is, a low transition density at the core crust boundary results in the crustal moment of inertia making up a higher fraction of the total.

In the left and center panels of Fig. 11 we show also the probability distributions for the total moment of inertia and the crustal moment of inertia as a function of the transition density and pressure for a $1.338 M_\odot$ neutron star. We find negative correlations with the transition density and relatively weak correlations with the transition pressure. Physically, as the transition density increases, L decreases and the neutron star becomes more compact. Thus the moment of inertia

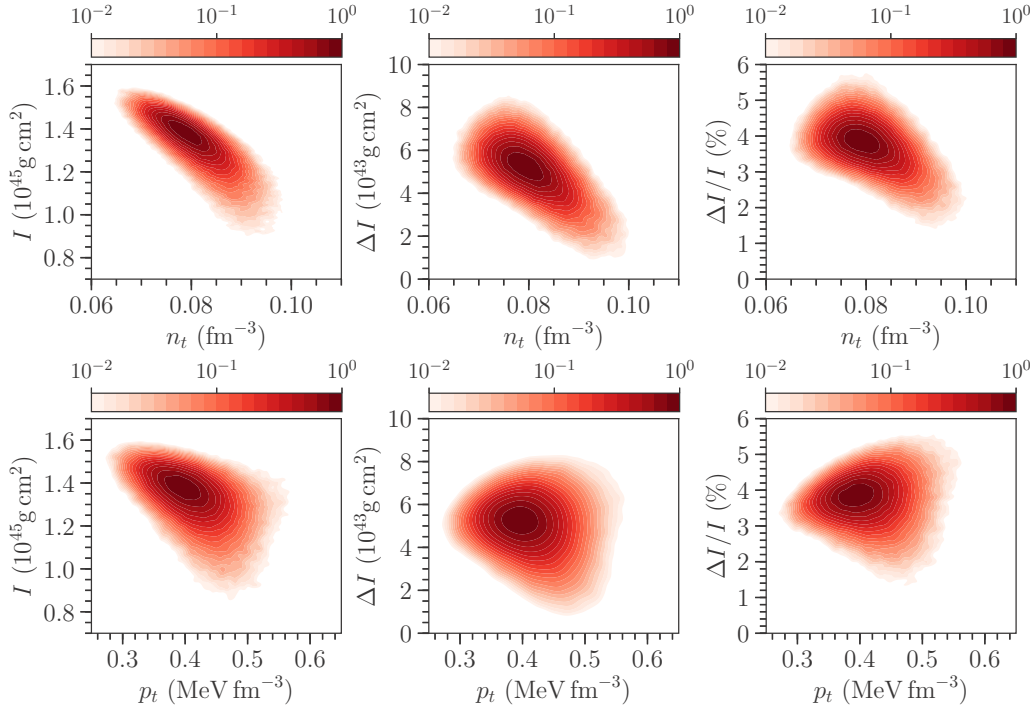

FIG. 11. Contour plots for the total moment of inertia I (left), crust moment of inertia ΔI (middle) and fractional crustal moment of inertia $\Delta I/I$ (right) vs. the transition density (top) and transition pressure (bottom) for a $M = 1.338\,M_\odot$ neutron star.

decreases. On the other hand, p_t is anticorrelated with I since p_t is anticorrelated with L and L correlates with R, the radius of the neutron star.

Since we find no strong link between the crustal moment of inertia and the core-crust transition pressure (in contrast to previous works), we examine in more detail the correlation between the transition pressure p_t and the core radius R_t, which was not considered in Refs. [53,54]. In Fig. 12 we plot the probability distribution of the core radius R_t^6 versus the core transition pressure. We find a statistically significant anticorrelation between the two quantities, which from Eq. (27) reduces the dependence of the crustal moment of inertia on the transition pressure. Indeed soft equations of state (with low values of L) are correlated with higher transition pressures as seen in Fig. 10 and also give rise to more compact neutron stars with smaller core radii. The combined result is almost no correlation between the crustal moment of inertia and the transition pressure, as seen in the middle panel of Fig. 11.

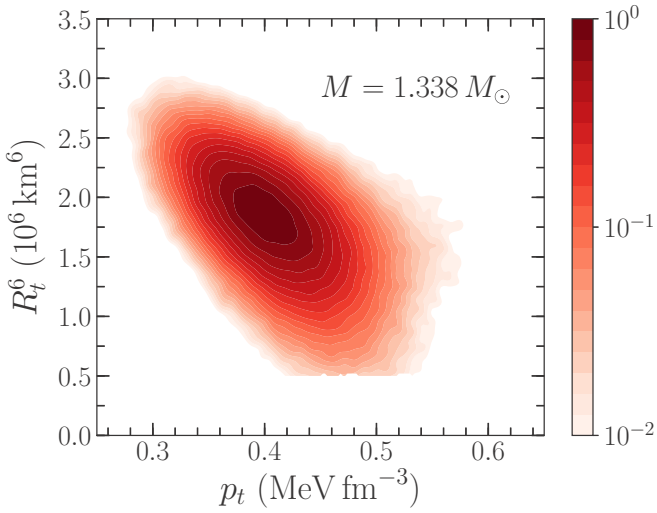

FIG. 12. Contour plot of the neutron star core radius R_t^6 vs. the crust-core transition pressure p_t for a $1.338\,M_\odot$ neutron star. We consider 300 000 equations of state generated from Bayesian modeling of the nuclear energy density functional.

V. SUMMARY

We have computed the moment of inertia of neutron stars based on a Bayesian analysis of the nuclear energy density functional constrained by chiral effective field theory and nuclear matter properties deduced from finite nuclei. We predict that for pulsar PSR J0737-3039A, with a well measured mass of $M = 1.338 M_\odot$, the moment of inertial lies in the range $1.04 \times 10^{45}\,\mathrm{g\,cm^2} < I < 1.51 \times 10^{45}\,\mathrm{g\,cm^2}$ at the 95% credibility level, while the most probable value for the moment of inertia is $\tilde{I} = 1.36 \times 10^{45}\,\mathrm{g\,cm^2}$. We have also shown that a pulsar timing measurement of the PSR J0737-3039A moment of inertia to 10% precision will result in meaningful constraints on the current Bayesian modeling of the equation of state by imposing the likelihood function for the posterior probability. Three scenarios were considered $I_{45} = \{1.1, 1.3, 1.5\}$ and the resulting effect on the neutron star mass-radius relation were analyzed. In particular, we find that the credibility interval for the radius of a $1.4\,M_\odot$ neutron

star decreases from $R_{+2\sigma} - R_{-2\sigma} = 2.6\,\mathrm{km}$ to 2.6, 1.8, and 1.6 km, depending on the moment of inertia measurement.

We have studied as well correlations among the neutron star moment of inertia, radius, and tidal deformability. A strong correlation is demonstrated between the moment of inertia and tidal deformability, indicating that one of the two quantities will strongly constrain the other. From our large sample of realistic equations of state, we derived a new functional model for the I/M^3 versus Λ universal relation.

Finally, we have employed realistic modeling of the crust equation of state to determine the fraction of the neutron star moment of inertia contained in the crust. We find that for typical neutron star masses of 1.2–1.5 $M_\odot$, the fractional crustal moment of inertia is less than 7%. In the strong neutron entrainment scenario, our small values of the crustal moment of inertia would be unable to account for the observed large glitch activity in the Vela pulsar. We have also shown that the crustal moment of inertia is weakly correlated with the core-crust transition density. Low transition densities at the core-crust boundary allow a large ratio between the moment of inertia of the neutron star crust to the total moment of inertia, since the high transition pressure is responsible for smaller core radii in neutron stars. In contrast to previous works, we find no correlation between the crustal moment of inertia and the transition pressure. It is understood that the symmetry energy slope parameter L is anticorrelated with p_t but positively correlated with R. Thus, their effects counteract each other, and no visible correlation is seen.

In the future we plan to incorporate as well neutron star radius measurements from the NICER mission and neutron star tidal deformability measurements the LIGO/VIRGO collaborations within the present Bayesian statistical modeling of the equation of state.

ACKNOWLEDGMENTS

This work was supported by the National Science Foundation under Grant No. PHY1652199. Portions of this research were conducted with the advanced computing resources provided by Texas A&M High Performance Research Computing.

[1] J. M. Lattimer and M. Prakash, Science **304**, 536 (2004).
[2] M. Burgay, N. D'Amico, A. Possenti, R. N. Manchester, A. G. Lyne, B. C. Joshi, M. A. McLaughlin, M. Kramer, J. M. Sarkissian, F. Camilo, V. Kalogera, C. Kim, and D. R. Lorimer, Nature **426**, 531 (2003).
[3] A. G. Lyne, M. Burgay, M. Kramer, A. Possenti, R. Manchester, F. Camilo, M. A. McLaughlin, D. R. Lorimer, N. D'Amico, B. C. Joshi, J. Reynolds, and P. C. C. Freire, Science **303**, 1153 (2004).
[4] J. M. Lattimer and B. F. Schutz, Astrophys. J. **629**, 979 (2005).
[5] N. Wex, Class. Quant. Gravity **12**, 983 (1995).
[6] T. Damour and G. Schäfer, Nuovo Cimento **101**, 127 (1988).
[7] B. P. Abbott *et al.* (LIGO Scientific Collaboration and Virgo Collaboration), Phys. Rev. Lett. **119**, 161101 (2017).
[8] B. P. Abbott *et al.* (The LIGO Scientific Collaboration and the Virgo Collaboration), Phys. Rev. Lett. **121**, 161101 (2018).
[9] A. L. Watts *et al.*, Rev. Mod. Phys. **88**, 021001 (2016).
[10] G. Baym, Phys. Rev. Lett. **30**, 1340 (1973).
[11] C.-K. Au and G. Baym, Nucl. Phys. A **236**, 500 (1974).
[12] N. K. Glendenning, Phys. Lett. B **114**, 392 (1982).
[13] N. K. Glendenning and S. A. Moszkowski, Phys. Rev. Lett. **67**, 2414 (1991).
[14] V. Thorsson, M. Prakash, and J. M. Lattimer, Nucl. Phys. A **572**, 693 (1994).
[15] N. K. Glendenning and J. Schaffner-Bielich, Phys. Rev. Lett. **81**, 4564 (1998).
[16] J. K. Bunta and S. Gmuca, Phys. Rev. C **70**, 054309 (2004).
[17] F. Weber, Prog. Part. Nucl. Phys. **54**, 193 (2005).
[18] M. Alford, M. Braby, M. Paris, and S. Reddy, Astrophys. J. **629**, 969 (2005).
[19] G. E. Brown, J. W. Holt, C.-H. Lee, and M. Rho, Phys. Rep. **439**, 161 (2007).
[20] G. E. Brown, C.-H. Lee, and M. Rho, Phys. Rep. **462**, 1 (2008).
[21] S. Weissenborn, I. Sagert, G. Pagliara, M. Hempel, and J. Schaffner-Bielich, Astrophys. J. **740**, L14 (2011).
[22] S. Weissenborn, D. Chatterjee, and J. Schaffner-Bielich, Nucl. Phys. **A881**, 62 (2012).
[23] S. Weissenborn, D. Chatterjee, and J. Schaffner-Bielich, Phys. Rev. C **85**, 065802 (2012).
[24] Y. Lim, K. Kwak, C. H. Hyun, and C.-H. Lee, Phys. Rev. C **89**, 055804 (2014).
[25] Y. Lim, C. H. Hyun, K. Kwak, and C.-H. Lee, Int. J. Mod. Phys. E **24**, 1550100 (2015).
[26] Y. Lim, C.-H. Lee, and Y. Oh, Phys. Rev. D **97**, 023010 (2018).
[27] P. Landry and B. Kumar, Astrophys. J. **868**, L22 (2018).
[28] T. Mølnvik and E. Østgaard, Nucl. Phys. A **437**, 239 (1984).
[29] I. A. Morrison, T. W. Baumgarte, S. L. Shapiro, and V. R. Pandharipande, Astrophys. J. **617**, L135 (2004).
[30] M. Bejger, T. Bulik, and P. Haensel, Mon. Not. R. Astron. Soc. **364**, 635 (2005).
[31] J. Piekarewicz, F. J. Fattoyev, and C. J. Horowitz, Phys. Rev. C **90**, 015803 (2014).
[32] T. Carreau, F. Gulminelli, and J. Margueron, arXiv:1810.00719.
[33] C. A. Raithel, F. Özel, and D. Psaltis, Astrophys. J. **831**, 44 (2016).
[34] C. A. Raithel, F. Özel, and D. Psaltis, Astrophys. J. **844**, 156 (2017).
[35] Y. Lim and J. W. Holt, Phys. Rev. Lett. **121**, 062701 (2018).
[36] L. Coraggio, J. W. Holt, N. Itaco, R. Machleidt, and F. Sammarruca, Phys. Rev. C **87**, 014322 (2013).
[37] L. Coraggio, J. W. Holt, N. Itaco, R. Machleidt, L. E. Marcucci, and F. Sammarruca, Phys. Rev. C **89**, 044321 (2014).
[38] F. Sammarruca, L. Coraggio, J. W. Holt, N. Itaco, R. Machleidt, and L. E. Marcucci, Phys. Rev. C **91**, 054311 (2015).
[39] J. W. Holt and N. Kaiser, Phys. Rev. C **95**, 034326 (2017).
[40] S. Weinberg, Physica A **96**, 327 (1979).
[41] D. R. Entem and R. Machleidt, Phys. Rev. C **68**, 041001(R) (2003).
[42] E. Epelbaum, H.-W. Hammer, and Ulf-G. Meißner, Rev. Mod. Phys. **81**, 1773 (2009).
[43] R. Machleidt and D. R. Entem, Phys. Rep. **503**, 1 (2011).

[44] E. Epelbaum, H. Krebs, and U.-G. Meißner, Phys. Rev. Lett. **115**, 122301 (2015).
[45] D. R. Entem, R. Machleidt, and Y. Nosyk, Phys. Rev. C **96**, 024004 (2017).
[46] M. Dutra, O. Lourenco, J. S. Sá Martins, A. Delfino, J. R. Stone, and P. D. Stevenson, Phys. Rev. C **85**, 035201 (2012).
[47] J. W. Holt and Y. Lim, Phys. Lett. B **784**, 77 (2018).
[48] N. Chamel, Phys. Rev. C **85**, 035801 (2012).
[49] N. Andersson, K. Glampedakis, W. C. G. Ho, and C. M. Espinoza, Phys. Rev. Lett. **109**, 241103 (2012).
[50] N. Chamel, A. F. Fantina, J. M. Pearson, and S. Goriely, Astron. Astrophys. **553**, A22 (2013).
[51] G. Watanabe and C. J. Pethick, Phys. Rev. Lett. **119**, 062701 (2017).
[52] J. M. Cordes, G. S. Downs, and J. Krause-Polstorff, Astrophys. J. **330**, 847 (1988).
[53] B. Link, R. I. Epstein, and J. M. Lattimer, Phys. Rev. Lett. **83**, 3362 (1999).
[54] F. J. Fattoyev and J. Piekarewicz, Phys. Rev. C **82**, 025810 (2010).
[55] K. Hebeler and A. Schwenk, Phys. Rev. C **82**, 014314 (2010).
[56] K. Hebeler, S. K. Bogner, R. J. Furnstahl, A. Nogga, and A. Schwenk, Phys. Rev. C **83**, 031301(R) (2011).
[57] A. Gezerlis, I. Tews, E. Epelbaum, S. Gandolfi, K. Hebeler, A. Nogga, and A. Schwenk, Phys. Rev. Lett. **111**, 032501 (2013).
[58] I. Tews, T. Krüger, K. Hebeler, and A. Schwenk, Phys. Rev. Lett. **110**, 032504 (2013).
[59] A. Roggero, A. Mukherjee, and F. Pederiva, Phys. Rev. Lett. **112**, 221103 (2014).
[60] A. Carbone, A. Rios, and A. Polls, Phys. Rev. C **90**, 054322 (2014).
[61] C. Drischler, V. Somà, and A. Schwenk, Phys. Rev. C **89**, 025806 (2014).
[62] G. Hagen, T. Papenbrock, A. Ekström, K. A. Wendt, G. Baardsen, S. Gandolfi, M. Hjorth-Jensen, and C. J. Horowitz, Phys. Rev. C **89**, 014319 (2014).
[63] G. Wlazłowski, J. W. Holt, S. Moroz, A. Bulgac, and K. J. Roche, Phys. Rev. Lett. **113**, 182503 (2014).
[64] C. Wellenhofer, J. W. Holt, and N. Kaiser, Phys. Rev. C **92**, 015801 (2015).
[65] I. Tews, S. Gandolfi, A. Gezerlis, and A. Schwenk, Phys. Rev. C **93**, 024305 (2016).
[66] C. Drischler, A. Carbone, K. Hebeler, and A. Schwenk, Phys. Rev. C **94**, 054307 (2016).
[67] F. Sammarruca, L. E. Marcucci, L. Coraggio, J. W. Holt, N. Itaco, and R. Machleidt, arXiv:1807.06640.
[68] K. Hebeler, J. M. Lattimer, C. J. Pethick, and A. Schwenk, Phys. Rev. Lett. **105**, 161102 (2010).
[69] K. Hebeler, J. M. Lattimer, C. J. Pethick, and A. Schwenk, Astrophys. J. **773**, 11 (2013).
[70] I. Tews, J. Carlson, S. Gandolfi, and S. Reddy, Astrophys. J. **860**, 149 (2018).
[71] P. Bedaque and A. W. Steiner, Phys. Rev. Lett. **114**, 031103 (2015).
[72] Y. Lim and J. W. Holt, arXiv:1902.05502 (2019).
[73] M. G. Alford, S. Han, and M. Prakash, Phys. Rev. D **88**, 083013 (2013).
[74] S. Han and A. W. Steiner, Phys. Rev. D **99**, 083014 (2019).
[75] J. W. Holt and Y. Lim, in *Xiamen-Custipen Workshop on the Equation of State of Dense Neutron-Rich Matter in the Era of Gravitational Wave Astronomy*, edited by A. Li, B.-A. Li, and F. Xu, AIP Conf. Proc. No. 2127 (AIP, Melville, 2019), p. 020019.
[76] J. M. Lattimer and Y. Lim, Astrophys. J. **771**, 51 (2013).
[77] I. Tews, J. M. Lattimer, A. Ohnishi, and E. E. Kolomeitsev, Astrophys. J. **848**, 105 (2017).
[78] J. Margueron and F. Gulminelli, Phys. Rev. C **99**, 025806 (2019).
[79] M. Kortelainen, T. Lesinski, J. Moré, W. Nazarewicz, J. Sarich, N. Schunck, M. V. Stoitsov, and S. Wild, Phys. Rev. C **82**, 024313 (2010).
[80] Y. Lim, C. H. Hyun, and C.-H. Lee, Int. J. Mod. Phys. E **26**, 1750015 (2017).
[81] J. M. Lattimer and F. D. Swesty, Nucl. Phys. A **535**, 331 (1991).
[82] Y. Lim and J. W. Holt, Phys. Rev. C **95**, 065805 (2017).
[83] J. B. Hartle, Astrophy. J. **150**, 1005 (1967).
[84] J. M. Lattimer and M. Prakash, Astrophys. J. **550**, 426 (2001).
[85] K. Yagi and N. Yunes, Phys. Rev. D **88**, 023009 (2013).
[86] W. C. G. Ho, C. M. Espinoza, D. Antonopoulou, and N. Andersson, Sci. Adv. **1**, e1500578 (2015).